

Inference of multi-channel r-process element enrichment in the Milky Way using binary neutron star merger observations

HSIN-YU CHEN,¹ PHILIPPE LANDRY,² JOCELYN S. READ,³ AND DANIEL M. SIEGEL^{4,5}

¹*Department of Physics, University of Texas at Austin, Austin, Texas 78712, USA*

²*Canadian Institute for Theoretical Astrophysics, University of Toronto, Toronto, ON M5S 3H8, Canada*

³*Department of Physics, California State University Fullerton, Fullerton, CA, USA*

⁴*Institute of Physics, University of Greifswald, D-17489 Greifswald, Germany*

⁵*Department of Physics, University of Guelph, Guelph, Ontario N1G 2W1, Canada*

ABSTRACT

Observations of GW170817 strongly suggest that binary neutron star (BNS) mergers can produce rapid neutron-capture nucleosynthesis (r-process) elements. However, it remains an open question whether BNS mergers can account for all the r-process element enrichment in the Milky Way’s history. Here we demonstrate that a BNS population model informed by multimessenger neutron star observations predicts a merger rate and per-event r-process element yield consistent with geophysical and astrophysical abundance constraints. If BNS mergers are to explain the r-process enrichment of stars in the Galaxy, we further show using a one-zone Galactic chemical evolution model that they have to merge shortly after the formation of their progenitors, with a delay time distribution of power-law index $\alpha \leq -2.0$ and minimum delay time $t_{\min} \leq 40$ Myr at 90% confidence. Such short delay times are in tension with those predicted by standard BNS formation models and those observationally inferred from samples of short gamma-ray bursts (sGRBs). However, we find that a two-channel enrichment scenario, where the second channel follows the star formation history, can account for both Galactic stellar and sGRB observations. Our results suggest that 45–90% of the r-process abundance in the Milky Way today was produced by a star-formation-tracking channel, rather than BNS mergers with significant delay times.

1. INTRODUCTION

A fundamental question of nuclear astrophysics is the origin of the elements in the solar system, the Milky Way, and the Universe as a whole. While it is relatively well-understood how elements up to iron are forged in the cores of stars and ejected through supernovae to enrich the metallicity of future stellar generations, the origins of the rapid neutron-capture (‘r-process’) elements, which must be produced in dense neutron-rich environments, remains open to active discussion (Cowan et al. 2021; Siegel 2022; Arcones & Thielemann 2022).

Observational constraints from various astrophysical environments tell us the characteristics of the events

that contribute r-process elements to our Universe. Geophysical constraints (Wallner et al. 2015; Hotokezaka et al. 2015) as well as observed levels and scatter of r-process elements in metal-poor stars in different environments, such as the Galactic halo (Macias & Ramirez-Ruiz 2018), ultra-faint dwarf galaxies (Ji et al. 2016; Beniamini et al. 2016), and globular clusters (Roederer & Sneden 2011; Roederer et al. 2016), suggest that they must be rare but prolific events in both recent and early Galactic history. For a summary and discussion of rate-yield constraints, see, e.g., Hotokezaka et al. (2018) and Siegel (2019). Observed abundances of r-process tracer elements such as Europium relative to stellar metallicity over the history of iron enrichment by supernovae, from the metal-poor stars of the Galactic halo to the high-metallicity environments of Galactic disk stars, suggest a significant, if not dominant, fraction of Galactic r-process events must have a short delay time with respect to star formation (Matteucci et al. 2014; Wehmeyer et al. 2015; Hotokezaka et al. 2018; Siegel 2019; Siegel et al. 2019; Côté et al. 2019; Lian et al. 2023; Van Der Swael-

hsinyu@austin.utexas.edu

plandry@cita.utoronto.ca

jread@fullerton.edu

daniel.siegel@uni-greifswald.de

men et al. 2023), although this has been questioned (Banerjee et al. 2020; Tarumi et al. 2021). Furthermore, the brief star formation histories in (ultra-faint) dwarf galaxies of only $\mathcal{O}(100\text{Myr})$ and of $\mathcal{O}(10\text{Myr})$ in globular clusters also require very short delay times for internal r-process enrichment (Ji et al. 2016; Skúladóttir et al. 2019; Naidu et al. 2022; Zevin et al. 2019; Kirby et al. 2020, 2023).

However, when evaluating candidate channels for r-process contributions in various environments, it has often been assumed that the overall rate of events, the amount of r-process element-containing ejected matter from each event (the ‘yield’), and the delay with respect to star formation are largely unconstrained and can be tuned to the levels required by abundance observations. With the advent of gravitational-wave (GW) astronomy establishing binary neutron star mergers as one site for r-process nucleosynthesis via GW170817, and with subsequently improving constraints on merging neutron star population properties (Abbott et al. 2017a), this is no longer true for neutron star mergers. In this work, we bring together several lines of observational evidence to quantitatively constrain the contribution of binary neutron star (BNS) merger events to r-process nucleosynthesis.

First, we make use of direct constraints on the rates and properties of BNS mergers from LIGO-Virgo-KAGRA (LVK) observations over the first three observing runs (The LIGO Scientific Collaboration et al. 2021; Abbott et al. 2023). Past results (e.g., Hotokezaka et al. (2018); Siegel (2019); Côté et al. (2019)) focus on the rate estimates made immediately after the first observation of a BNS merger GW170817 (Abbott et al. 2017a), which assumed that all BNS mergers have similar properties. Additional events, and (thanks to a well-modeled sensitive volume over the following observing runs) observing time without events, however, furthered our understanding of the merger population as a whole. GW astronomy is now producing rate estimates as a function of component masses, which extend beyond the point-observation of GW170817 (Abbott et al. 2019).

Second, we make use of constraints coming from observations of AT 2017gfo (Abbott et al. 2017b) associated with GW170817, the first direct observation of an r-process enrichment event consistent with a kilonova (Metzger et al. 2010; Metzger 2020). These observations infer the amount of r-process material produced and thus inform models based on numerical relativity simulations of the merger and postmerger phase to predict the amount of r-process ejected by a given BNS system for a given equation of state (EOS) (Krüger & Foucart 2020; Nedora et al. 2021). To explain the ob-

served GW170817 kilonova requires taking into account not only ejecta contributions from the dynamical merger phase (Rosswog et al. 1999; Ruffert et al. 1997; Oechslin et al. 2007; Hotokezaka et al. 2013), but also from the postmerger phase in the form of neutrino and magnetically driven winds (Dessart et al. 2008; Perego et al. 2014; Desai et al. 2022; Siegel et al. 2014; Cioffi et al. 2017; Metzger et al. 2018; Combi & Siegel 2023; Curtis et al. 2024) from a remnant neutron star and disk winds (Metzger et al. 2008; Fernández & Metzger 2013; Just et al. 2015; Siegel & Metzger 2017; Fernández et al. 2019; Combi & Siegel 2023; Kiuchi et al. 2023) from a postmerger accretion disk (see, e.g., Metzger (2020); Siegel (2019, 2022); Margutti & Chornock (2021); Pian (2021); Radice et al. (2020) for a discussion). As carried out in Chen et al. (2021); De & Siegel (2021); Siegel (2022), modern simulations predict the contributions through most of these outflows from the component masses of each merger and the neutron-star EOS.

Third, we take a data-driven posterior distribution for the neutron-star EOS at high density, which combines information from an array of astronomical observations of neutron stars. Here, we use the public EOS posterior samples of Legred et al. (2021), which are informed by pulsar mass measurements, GW observations, and X-ray pulse profile modeling. The EOS constraints encoded in this posterior distribution are broadly consistent with those of e.g. Huth et al. (2022); Capano et al. (2020), which include additional astrophysical and nuclear-physics constraints.

Fourth, we take an empirical estimate for the delay time distribution of neutron-star mergers that comes from the observations of the galaxy offsets of short gamma-ray bursts (sGRBs) (Zevin et al. 2022). This provides limits on the distribution of delay times for merger events, assuming that sGRB associations are an unbiased probe of the merging BNS population. Notably, the power-law slope of the sGRB-inferred delay time distribution is steeper than the conventional expectation of $\alpha \approx -1$ for BNSs formed through isolated binary evolution (Piran 1992; Dominik et al. 2012; Mapelli & Giacobbo 2018; Neijssel et al. 2019).

Together, these results have quantitative implications for the amount of r-process elements that will be contributed by BNS mergers. We produce four key results:

(1) We estimate the r-process ejecta mass and rate distributions from BNS mergers, as constrained by the observational results mentioned above, and update the comparison of Hotokezaka et al. (2018) and Siegel (2019). We show that the predicted rates and yields overlap with geophysical and astrophysical constraints.

(2) We use a one-zone Galactic chemical evolution model of nucleosynthesis from both supernovae and BNS mergers with the observed rates, masses, EOS, and delay times to derive a distribution of predicted tracks through the relative abundance history of $[\text{Fe}/\text{H}]$ to $[\text{Eu}/\text{Fe}]$ (Siegel et al. 2019). As expected, this single-site model does not suffice to generate the amount of Europium enrichment observed at low metallicity. However, as seen in (1), the observed contribution from merger events can quantitatively reproduce the relative abundances observed at solar metallicity. We note that current uncertainties are large, so this does not yet exclude additional significant channels.

(3) We consider what delay-time distribution would be required, instead of the one suggested by sGRBs observations, to reproduce both the Europium abundance at solar metallicity and the changing abundances at lower metallicity. As expected, the significant contribution at low metallicity requires shorter delay times than those inferred from sGRBs.

(4) Starting with the observation-based estimates of the contributions from BNS mergers and retaining the sGRB-inferred delay times, we constrain the overall yield of r-process contribution of a second channel as needed to make up the difference between the contributions of BNS mergers and the observations of high-metallicity disk stars with $[\text{Fe}/\text{H}] \gtrsim -1$.

2. BINARY NEUTRON STAR R-PROCESS PRODUCTION RATE AND YIELD

The r-process enrichment event rate and per-event yield have been constrained by astrophysical and geological measurements. In order to test whether BNS mergers are consistent with these constraints, we use LVK observations to estimate the BNS merger rate, and analytical fits to numerical simulations to estimate the average amount of r-process ejecta per merger event.

- *Local merger rate:* We use the BNS population distribution inferred from the LVK’s GWTC-3 catalog (The LIGO Scientific Collaboration et al. 2021). Specifically, we adopt the **Power Law + Dip + Break** population model from Abbott et al. (2023); other population model choices in that study predict consistent merger rates. Abbott et al. (2023) provides 1501 posterior rate samples binned in mass. For every rate sample, we sum the rate density over mass bins up to the maximum mass for a given neutron star EOS sample and convert the resulting BNS merger rate to a Galactic event rate, R_{MW} , assuming a number density of Milky-Way like galaxies of 0.01 Mpc^{-3} .

- *Neutron star equation of state:* The amount of ejecta produced by a BNS merger depends sensitively on the neutron star EOS. Although the high-density EOS is still uncertain, astronomical observations and recent developments based on chiral effective field theory and many-body perturbation theory in nuclear theory (e.g., Drischler et al. 2020) have started to constrain and quantify the uncertainties. Legred et al. (2021) conditioned a phenomenological Gaussian process model for the EOS on X-ray, radio, and GW observations of neutron stars to provide a set of posterior EOS samples and corresponding neutron star mass-radius relations. For every merger rate sample, we randomly pick a mass-radius relation sample from this set to map from neutron star component masses (m_1, m_2) to radii (R_1, R_2) .
- *Ejecta mass estimate:* We estimate ejecta mass per event, m_{ej} , following the approach in Chen et al. (2021):

$$m_{\text{ej}} = \alpha_{\text{dyn}} m_{\text{dyn}} + f_{\text{loss}} m_{\text{disk}},$$

where m_{dyn} represents the mass of the dynamical ejecta, and m_{disk} the mass of the disk formed in the postmerger phase. In order to estimate m_{dyn} and m_{disk} , we use analytical fits to numerical simulations in Krüger & Foucart (2020)—specifically, their Eq. (6) for the dynamical ejecta and Eq. (4) for the disk—which depend on the mass and radius of the component neutron stars. The coefficient α_{dyn} is a scaling factor which is randomly sampled between $[0.5, 1.5]$ to account for an uncertainty of 50% in the knowledge of m_{dyn} . The fraction f_{loss} of mass ejected from the disk is randomly sampled between $[0.15, 1]$ to account for its uncertainty.

Given these three prescriptions, for each rate and EOS sample, we sample uniformly in component masses (m_1, m_2) up to the maximum neutron star mass, estimate the ejecta mass for each of these BNS realizations, and perform a rate-density-weighted sum over BNS realizations to obtain the average ejecta mass per event.

In Fig. 1, we show the inferred BNS merger rate as a function of average ejecta mass per event. The r-process production rate and yield for BNS mergers is consistent with constraints from the total stellar mass in the Milky Way (McMillan 2011), metal-poor stars (Macias & Ramirez-Ruiz 2018), dwarf galaxies (Beniamini et al. 2016), and ^{244}Pu measurements (Hotokezaka et al. 2015).

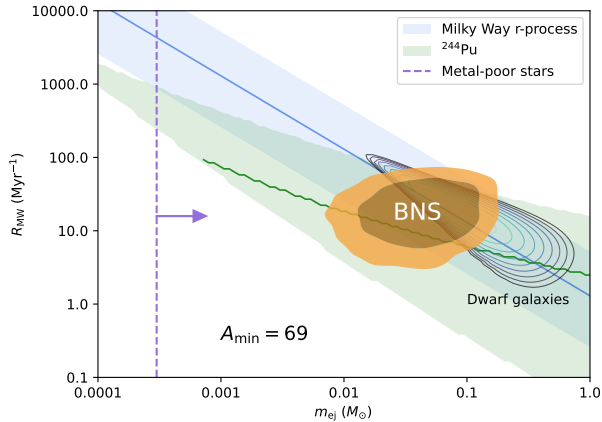


Figure 1. BNS event rate per Milky Way like galaxy as a function of average ejecta mass per event. The dark and light orange shades are the 68% and 90% confidence intervals. We over plot the constraints from total stellar mass in Milky Way (McMillan (2011), blue band), metal-poor stars (Macias & Ramirez-Ruiz (2018), purple, lower limit), dwarf galaxies (Beniamini et al. (2016), grey contours), and ^{244}Pu measurements (Hotokezaka et al. (2015), green band). We assume an r-process with the solar abundance pattern for atomic mass number $A \geq 69$.

3. CHEMICAL ABUNDANCE EVOLUTION

Although the BNS merger rate and average ejecta mass is consistent with existing constraints at $z = 0$, a different picture may emerge when enrichment is viewed as a function of cosmic time in various environments and in the context of chemical evolution including other metals. The observed abundances of r-process tracer elements like Eu as a function of stellar metallicity $[\text{Fe}/\text{H}]$ record the r-process element enrichment at different stages of Milky Way evolution. The r-process enrichment history associated with the BNS merger channel depends on its rate evolution, which can be expressed in terms of a star formation rate convolved with a distribution of delay times measuring the lag between the formation of the progenitor system and the merger. In order to examine whether BNS mergers can produce the measured stellar abundances, we use sGRB observations to inform the BNS delay time distribution and adopt a one-zone model to estimate chemical abundances over time.

- *Delay time distribution from short gamma-ray bursts:* The BNS merger rate inferred from GWs is confined to the local Universe, and the evolution of the merger rate across cosmic history is currently beyond the sensitivities of the LVK observatories. However, observations of EM counterparts of BNS mergers, such as sGRBs, can provide insight into the merger rate at higher redshift, assuming they

appropriately sample the merging BNS distribution. Using 68 identified host galaxies of sGRBs, Zevin et al. (2022) constrained the sGRB rate evolution. Specifically, the rate of sGRBs at cosmic age t can be written as

$$R_{\text{sGRB}}(t) = C_{\text{sGRB}} \int_0^t D(t-t' | t_{\text{min}}, t_{\text{max}}, \alpha) \Psi_{\text{SFH}}(t') dt',$$

where $\Psi_{\text{SFH}}(t)$ represents the Galactic star formation rate per unit time; we assume the Galactic star formation history follows the cosmic star formation history (Madau & Fragos 2017). The normalization factor C_{sGRB} is calibrated by the observed local sGRB rate. The delay time distribution (DTD)

$$D(t | t_{\text{min}}, t_{\text{max}}, \alpha) \propto t^\alpha, \quad t_{\text{min}} \leq t \leq t_{\text{max}} \quad (1)$$

describes the time between the formation of the progenitor stars and the onset of sGRBs. Zevin et al. (2022) found a relatively steep power-law index of $\alpha = -1.83^{+0.35}_{-0.39}$ and a long minimum delay time of $t_{\text{min}} = 184^{+67}_{-79}$ Myr. No strong constraint could be placed on t_{max} . We assume t_{max} to be the current age of the Universe. While this is not a strong assumption for our modelling, we do know of BNS systems that have a longer inspiral time than the age of the Universe. Although it is uncertain whether sGRBs are representative of the entire population of BNS mergers, the sGRB population is still one of the best indicators of the evolution of the BNS merger rate. Therefore, we use the local BNS merger rate C_{BNS} inferred from LVK observations (Abbott et al. 2023) to calibrate Eq. (1) instead of C_{sGRB} and project the BNS rate $R_{\text{BNS}}(t)$ over time.

- *One-zone model:* We describe the Galactic production of iron-peak and r-process elements over cosmic time using the one-zone chemical evolution model of Siegel et al. (2019). One-zone models assume instantaneous homogeneous mixing of metals in the interstellar medium (ISM), and thus cannot adequately capture effects of hierarchical structure growth and inhomogeneities due to incomplete mixing associated with rare enrichment events at low metallicity. However, they can accurately capture the average enrichment levels of the ISM with r-process elements at high metallicity, once the ISM has been polluted by a significant number of individual events. We use the same Galactic in- and outflow rate and the same rates

and yields for iron production by core-collapse and Type Ia supernovae as in Siegel et al. (2019), while we adjust the rate and yield of r-process enrichment as traced by Eu according to the local merger rate, DTD, and ejecta mass estimates discussed above. The total r-process ejecta mass per event is translated into a Eu mass per event by assuming a solar abundance distribution of r-process elements (Arnoult et al. 2007) starting at atomic mass number $A = 69$. Representing the cumulative total over many individual enrichment events and a rough average to the r-process abundance patterns of many individual observations of r-process enhanced metal-poor stars that have been polluted by a single or only by a few r-process events (e.g. Frebel & Ji 2023), the solar r-process abundance pattern provides a reasonable estimate for average r-process enrichment at high metallicity.

We first consider an r-process enrichment scenario in which BNS mergers with an sGRB-informed DTD are the only enrichment site. Fig. 2 shows the abundance ratio of $[\text{Eu}/\text{Fe}]$ as a function of $[\text{Fe}/\text{H}]$. We overplot the observed metallicities of Galactic disk stars from Battistini & Bensby (2016) (blue diamonds), as well as observations from the Stellar Abundances for Galactic Archaeology (SAGA) database (Suda et al. 2011; green crosses), which span both metal-rich disk stars and metal-poor halo stars. Despite the large statistical uncertainty originating from the uncertainties in BNS merger rate (locally and at higher redshift), mass distribution, neutron star EOS, and analytic fits to ejecta in numerical simulations as described in the previous section, the abundance ratio $[\text{Eu}/\text{Fe}]$ estimated from the BNS-only model shows a clear deviation from the stellar observations at low metallicity. Thus, while this single-site model can match the observed Eu abundance at $z = 0$, it cannot reproduce the Galactic history of r-process enrichment.

4. BINARY NEUTRON STAR DELAY TIMES INFERRED FROM MILKY WAY DISK STARS

We showed above that BNS mergers alone cannot match the Galactic stellar observations that probe Milky Way chemical abundance history, given reasonable assumptions about their astrophysical rate, population, delay time distribution and EOS. We now relax these astrophysical assumptions and ask what it would take for BNS mergers to reproduce the history of r-process chemical evolution in the Galaxy. Fig. 2 shows that the median of the predicted $[\text{Eu}/\text{Fe}]$ abundance ratio is consistent with stellar observations around solar metallicity

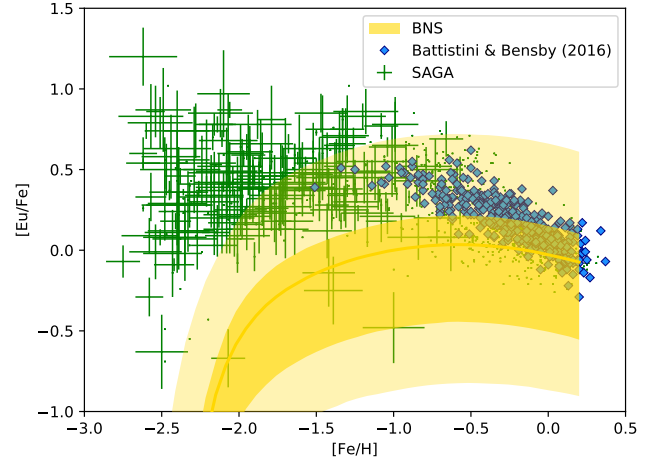


Figure 2. The abundance ratio $[\text{Eu}/\text{Fe}]$ as a function of metallicity $[\text{Fe}/\text{H}]$ assuming BNS mergers as the only r-process element production site. The yellow line is the median. The dark and light bands are the 68% and 90% confidence intervals. We also overplot the Galactic stellar observations taken from Battistini & Bensby (2016) (blue diamonds) and the SAGA database (Suda et al. (2011); green crosses).

($[\text{Fe}/\text{H}] \gtrsim 0.0$), but that the deviation grows with decreasing metallicity. Among the sources of uncertainty, the local merger rate, mass distribution, and neutron star EOS affect the overall abundances of r-process elements, i.e., the vertical offset in Fig. 2. On the other hand, the slope of $[\text{Eu}/\text{Fe}]$ as a function of $[\text{Fe}/\text{H}]$ is dominated by the merger rate evolution over time. Therefore, instead of using the delay time distribution informed by sGRBs, we try to determine the BNS DTD that could explain the observed trend of r-process abundances.

We model each stellar measurement of $[\text{Eu}/\text{Fe}]$ and $[\text{Fe}/\text{H}]$ as a two-dimensional Gaussian likelihood function $P(d_i | [\text{Eu}/\text{Fe}], [\text{Fe}/\text{H}])$ with zero covariance. Our results are conditioned on the Battistini & Bensby (2016) disk stars only, as the one-zone chemical evolution model is strictly valid solely at high metallicities when the interstellar medium has already been enriched by many r-process events and there exist well-defined average r-process abundances. The width of the Gaussian likelihood function is dictated by the average standard deviations quoted in Battistini & Bensby (2016).

Within the one-zone model connecting a BNS population to an r-process abundance history, we sample randomly in local ($z = 0$) BNS rate-yield ($m_{\text{ej}} R_{\text{MW}}$) and DTD parameters (t_{min}, α) and calculate the corresponding $[\text{Eu}/\text{Fe}]$ vs $[\text{Fe}/\text{H}]$ track. All other population parameter uncertainties—such as those in the NS mass distribution and EOS—are implicitly marginalized over

in determining the distribution of possible BNS merger rates and yields. The likelihood of the local BNS rate-yield and DTD parameters is then given by

$$P(d|t_{\min}, \alpha, m_{\text{ej}}R_{\text{MW}}) = \prod_i \int d[\text{Eu}/\text{Fe}]d[\text{Fe}/\text{H}]P(d_i|[\text{Eu}/\text{Fe}], [\text{Fe}/\text{H}]) \times P([\text{Eu}/\text{Fe}], [\text{Fe}/\text{H}]|t_{\min}, \alpha, m_{\text{ej}}R_{\text{MW}}),$$

where the product is taken over all the stellar spectrum measurements and $P([\text{Eu}/\text{Fe}], [\text{Fe}/\text{H}]|t_{\min}, \alpha, m_{\text{ej}}R_{\text{MW}})$ is a delta-function likelihood located along the r-process abundance track prediction of the model with DTD parameters (t_{\min}, α) and local BNS rate-yield $m_{\text{ej}}R_{\text{MW}}$.

For this analysis, our prior is log-uniform for $t_{\min} \in [1, 2000]$ Myr and uniform for $\alpha \in [-3.0, -0.5]$. The prior on $m_{\text{ej}}R_{\text{MW}}$ is informed by the rate-yield posterior from Sec. 2. In practice, we evaluate Eq. (2) via numerical integration on a grid of points drawn along the $([\text{Eu}/\text{Fe}], [\text{Fe}/\text{H}])$ track for each sample in $(t_{\min}, \alpha, m_{\text{ej}}R_{\text{MW}})$.

As shown in Fig. 3, the disk-star data favor a very short minimum delay time, $t_{\min} \leq 40$ Myr at 90% confidence, with a steep delay time distribution, $\alpha \leq -2.0$. This is because the disk stars' Eu abundances decreases, on average, as a function of metallicity, mirroring the decline of the cosmic star formation rate for $z \lesssim 2$ together with increased Fe dilution due to SN Ia; this decreasing trend is difficult to reproduce with long-lived BNS systems.

The extremely short inferred BNS delay times are in clear tension with the sGRB-derived BNS DTD prediction of Zevin et al. (2022), which favors $t_{\min} \approx 180$ Myr and $\alpha \approx -1.8$ ¹. They are also inconsistent with the standard isolated binary evolution scenario for the formation of BNSs, which predicts $\alpha \approx -1.0$ (e.g., Piran 1992) and $t_{\min} \gtrsim 30$ Myr (e.g., Neijssel et al. 2019). This suggests that either the BNS population has a fast-merging subpopulation, or that BNS mergers are just one channel among multiple sites for r-process nucleosynthesis.

5. MULTI-CHANNEL R-PROCESS ENRICHMENT

As a way to resolve the tension between the sGRB observations and the BNS delay time distribution inferred from Galactic disk stars within the single-channel

¹ We note that the tension also applies to the DTD values discussed in other GRB studies (e.g., D'Avanzo et al. (2014); Wanderman & Piran (2015)). However, completeness of the sample is an issue and shorter average delay times may be possible (Salafia et al. 2023).

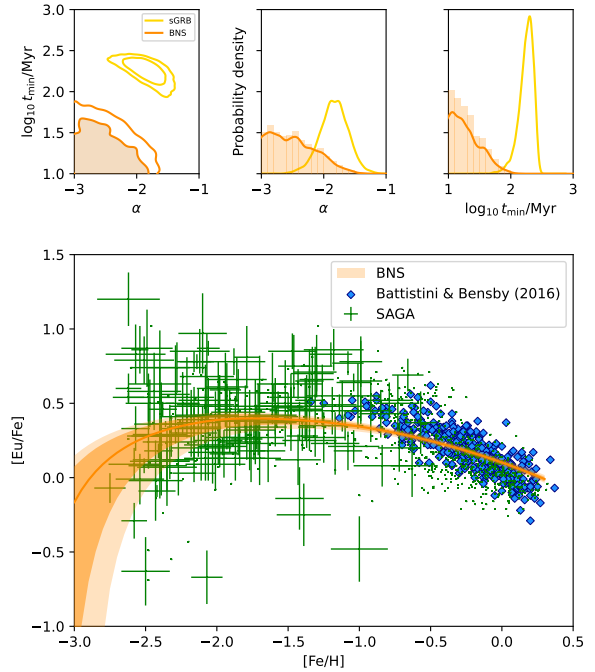


Figure 3. BNS delay time distribution parameters and $[\text{Eu}/\text{Fe}]$ to $[\text{Fe}/\text{H}]$ abundance ratio evolution (orange) inferred from Battistini & Bensby (2016)'s disk star observations, assuming that BNS mergers are the sole site of r-process nucleosynthesis. Contours and shading represent 68% and 90% confidence regions. The delay time distribution parameters inferred from short gamma-ray burst observations in Zevin et al. (2022) (yellow) are shown for comparison.

r-process model, we now assume a second r-process nucleosynthesis site that tracks the star formation history of the Milky Way but does not significantly contribute to the production of Fe. This updates the one-zone model for predicting the $[\text{Eu}/\text{Fe}]$ vs $[\text{Fe}/\text{H}]$ track, $P([\text{Eu}/\text{Fe}], [\text{Fe}/\text{H}]|t_{\min}, \alpha, X_{\text{SFH}}, m_{\text{ej}}R_{\text{MW}})$, with one more input parameter

$$X_{\text{SFH}} = \frac{\int m_{\text{SFH}} R_{\text{SFH}}(t) dt}{\int [m_{\text{SFH}} R_{\text{SFH}}(t) + m_{\text{ej}} R_{\text{BNS}}(t)] dt}, \quad (2)$$

the mass fraction of r-process abundance contributed by the second channel over Galactic history. Here, m_{SFH} is the per-event second-channel yield and $R_{\text{SFH}}(t)$ is its rate, in parallel to m_{ej} and $R_{\text{BNS}}(t)$ for the BNS channel.

We reanalyze the disk-star and SAGA observations with the sGRB-informed prior on t_{\min} and α , and the same prior on $m_{\text{ej}}R_{\text{MW}}$ as above, to constrain the second channel's contribution. We place a uniform prior on $X_{\text{SFH}} \in [0, 1]$. The results are presented in Fig. 4. The disk-star observations constrain the second channel's fractional contribution to be $X_{\text{SFH}} = 0.71^{+0.20}_{-0.25}$ of

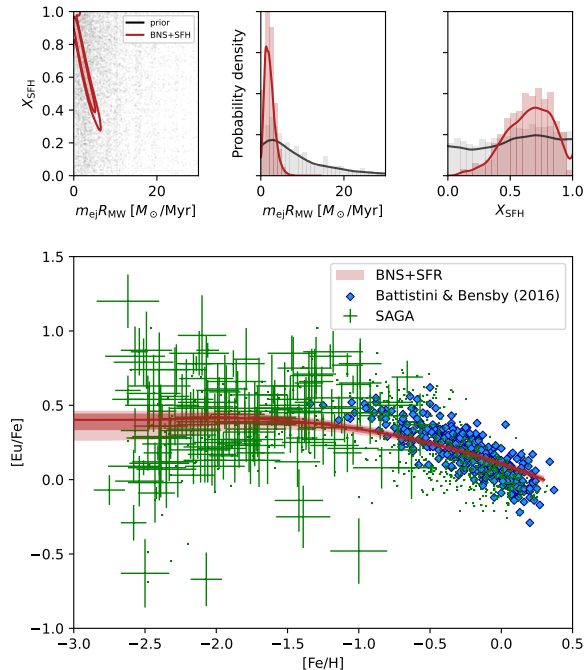


Figure 4. BNS r-process yield, second-channel contribution fraction by mass, and $[\text{Eu}/\text{Fe}]$ to $[\text{Fe}/\text{H}]$ abundance ratio evolution inferred from Battistini & Bensby (2016)’s disk star formation history-tracing channel contribute to r-process nucleosynthesis. The BNS delay time distribution is informed by short gamma-ray burst observations (Zevin et al. 2022). Contours and shading represent 68% and 90% confidence regions.

the integrated r-process abundance by mass. The disk-star data also tightly constrain the local BNS rate-yield to be $m_{\text{ej}}R_{\text{MW}} = 1.9^{+2.3}_{-1.4} M_{\odot}/\text{Myr}$. The Galactic stellar spectra do not constrain the BNS DTD relative to the sGRB prior within the multi-channel model. The good fit to the data in Fig. 4 demonstrates that a two-site model can reproduce Galactic stellar observations, whereas a sole-source BNS merger origin for r-process elements is inconsistent with the sGRB constraints on the DTD Zevin et al. (2022), as well as theoretical expectations for BNS delay times, as discussed above. The data prefer the two-channel model to the BNS-only model with a Bayes factor of $\sim 10^5$, computed as a Savage-Dickey density ratio of the two-channel posterior to the prior at $X_{\text{SFH}} = 0$, when the sGRB DTD is used as a prior. Remarkably, we find that the BNS merger channel and the star formation history-tracing channel have contributed at the same order of magnitude to the present-day r-process abundance in the Galaxy.

6. DISCUSSION

Our study of BNS mergers’ contribution to r-process element enrichment in the Milky Way across cosmic time combines data from multiple kinds of astrophysical observations. We constrain the BNS merger rate evolution required to explain Galactic stellar observations, and estimate the contribution from a second r-process channel.

Although BNS mergers’ rate and per event r-process element yield are consistent with astrophysical and geological measurements, a much shorter delay relative to star formation history is required for BNS mergers alone to account for the Galactic stellar $[\text{Eu}/\text{Fe}]$ observations at different metallicities. We therefore explore the possibility of a second r-process site with no significant time delay compared to star formation. Possible candidates for such a site include collapsars (Pruet et al. 2003; Surman et al. 2006; Fujimoto et al. 2007; Siegel et al. 2019) or MHD supernovae (Nishimura et al. 2006; Winteler et al. 2012; Nishimura et al. 2017; Halevi & Mösta 2018; Reichert et al. 2021). The second channel’s significant inferred fractional contribution of $0.71^{+0.20}_{-0.25}$ to the present-day Galactic r-process abundance is consistent with previous estimates for a collapsar channel (Siegel et al. 2019).

The second site could also be a separate subpopulation of BNSs. In our model, all BNS mergers follow the same rate evolution. However, Galactic observations of binary pulsars suggest that 40–60% of BNS systems merge rapidly (Beniamini & Piran 2019), and the massive BNS merger GW190425 has been interpreted to support a shorter time from formation to merger (Abbott et al. 2020; Romero-Shaw et al. 2020; Galadage et al. 2021). There is also theoretical support for a fast-merging BNS channel (Belczynski et al. 2002; Dewi & Pols 2003; Ivanova et al. 2003; Beniamini & Piran 2023). Moreover, there can be a subpopulation of sGRBs with shorter delay time (Nugent et al. 2024). Also, sGRB observations may not necessarily represent the entire BNS population, especially given recent evidence of a long GRB associated with a BNS (Rastinejad et al. 2022).

Neutron star-black hole mergers are another possible r-process site, although their contribution is highly dependent on their rate evolution and yield (Chen et al. 2021), the latter of which may be quite low based on current evidence (Biscoveanu et al. 2023). Despite the broad range of candidates for the second channel, our study places an initial constraint on the fractional contribution from this site (or combination of sites), besides typical BNS mergers.

Systematic uncertainties in the abundance data could quantitatively change our results. The assessment of the systematic uncertainty for the data we used was done by comparison with other measurements on overlap-

ping stars. With the 0.05–0.06 dex difference in the Eu abundance (reported as $\Delta[\text{Eu}/\text{H}]$ in Battistini & Bensby (2016)), we do not expect a significant change in our results. Furthermore, the late-time abundance trend of $[\text{Eu}/\text{Fe}]$ vs. $[\text{Fe}/\text{H}]$ is sensitive to the power-law index of the DTD of Type Ia supernovae. However, this index of -1.1 ± 0.1 has been consistently inferred both from direct measurement using galaxy clusters (Freundlich & Maoz 2021) and from measurement of Type Ia rates and the cosmic star formation history (Maoz & Graur 2017).

Various modeling uncertainties could also affect our results, e.g. the uncertainties in the amount of disk material ejected into disk winds in the postmerger phase (currently absent a set of long-term self-consistent simulations) and in the abundance distribution emerging from a given binary (i.e., the predicted Eu mass per event) due to uncertainties in both predicting the astrophysical conditions of the r-process and intrinsic nuclear uncertainties (Horowitz et al. 2019). Furthermore, there are open questions in reconciling kilonova observations and other constraints on the EOS (Kedia et al. 2023) and in understanding the heavy element production of nuclear reaction networks under the thermodynamic conditions of the outflows (Cowan et al. 2021). As observational constraints tighten, this modeling uncertainty will become more significant.

More detailed models for chemical evolution and star formation histories of the Milky Way will also improve the robustness of our results. In particular, they would

allow for the treatment of lower-metallicity halo star observations, which are impacted by inhomogeneities in the mixing of r-process elements in the ISM. Nonetheless, we do not expect these observations to alter our qualitative conclusions; even within the one-zone model, we find similar quantitative constraints on the BNS DTD, rate-yield and second-channel contribution when the halo- and disk-star SAGA observations (Suda et al. 2011) are used in place of the Battistini & Bensby (2016) disk star ones.

- 1 The authors would like to thank Alexander Ji, Om Sha-
- 2 ran Salafia, and Sharan Banagiri for useful discussions.
- 3 P.L. is supported by the Natural Sciences & Engineer-
- 4 ing Research Council of Canada. J.S.R. is supported
- 5 by NSF PHY-2110441. We thank the Institute for Nu-
- 6 clear Theory at the University of Washington for its kind
- 7 hospitality and stimulating research environment dur-
- 8 ing INT 20r-1b. This research was supported in part
- 9 by the INT’s U.S. Department of Energy grant No. DE-
- 10 FG02-00ER41132. The authors are grateful for com-
- 11 putational resources provided by the LIGO Laboratory
- 12 and supported by National Science Foundation Grants
- 13 PHY-0757058 and PHY-0823459. This material is based
- 14 upon work supported by NSF’s LIGO Laboratory which
- 15 is a major facility fully funded by the National Science
- 16 Foundation.

REFERENCES

- Abbott, B. P., Abbott, R., Abbott, T. D., & et al. 2017a, *PhRvL*, 119, 161101
- . 2017b, *ApJL*, 848, L12
- Abbott, B. P., et al. 2019, *Phys. Rev. X*, 9, 011001
- . 2020, *Astrophys. J. Lett.*, 892, L3
- Abbott, R., et al. 2023, *Phys. Rev. X*, 13, 011048
- Arcones, A., & Thielemann, F.-K. 2022, *The Astronomy and Astrophysics Review*, 31, 1
- Arnould, M., Goriely, S., & Takahashi, K. 2007, *PhR*, 450, 97
- Banerjee, P., Wu, M.-R., & Yuan, Z. 2020, *ApJL*, 902, L34
- Battistini, C., & Bensby, T. 2016, *A&A*, 586, A49
- Belczynski, K., Kalogera, V., & Bulik, T. 2002, *ApJ*, 572, 407
- Beniamini, P., Hotokezaka, K., & Piran, T. 2016, *ApJ*, 832, 149
- Beniamini, P., Hotokezaka, K., & Piran, T. 2016, *ApJ*, 832, 149
- Beniamini, P., & Piran, T. 2019, *Monthly Notices of the Royal Astronomical Society*, 487, 4847
- Beniamini, P., & Piran, T. 2023, arXiv e-prints, arXiv:2312.02269
- Biscoveanu, S., Landry, P., & Vitale, S. 2023, *MNRAS*, 518, 5298
- Capano, C. D., Tews, I., Brown, S. M., et al. 2020, *Nature Astronomy*, 4, 625
- Chen, H.-Y., Vitale, S., & Foucart, F. 2021, *ApJL*, 920, L3
- Ciolfi, R., Kastaun, W., Giacomazzo, B., & et al. 2017, *Physical Review D*, 95, 063016
- Combi, L., & Siegel, D. M. 2023, *Phys. Rev. Lett.*, submitted, arXiv:2303.12284
- Côté, B., Eichler, M., Arcones, A., & et al. 2019, *ApJ*, 875, 106
- Cowan, J. J., Sneden, C., Lawler, J. E., et al. 2021, *Reviews of Modern Physics*, 93, 015002
- Cowan, J. J., Sneden, C., Lawler, J. E., & et al. 2021, *Rev. Mod. Phys.*, 93, 015002

- Curtis, S., Bosch, P., Mösta, P., & et al. 2024, *ApJL*, 961, L26
- D’Avanzo, P., Salvaterra, R., Bernardini, M. G., et al. 2014, *MNRAS*, 442, 2342
- De, S., & Siegel, D. M. 2021, *The Astrophysical Journal*, 921, 94
- Desai, D., Siegel, D. M., & Metzger, B. D. 2022, *ApJ*, 931, 104
- Dessart, L., Ott, C. D., Burrows, A., & et al. 2008, *ApJ*, 690, 1681
- Dewi, J. D. M., & Pols, O. R. 2003, *MNRAS*, 344, 629
- Dominik, M., Belczynski, K., Fryer, C., et al. 2012, *ApJ*, 759, 52
- Drischler, C., Furnstahl, R. J., Melendez, J. A., & et al. 2020, *PhRvL*, 125, 202702
- Fernández, R., & Metzger, B. D. 2013, *MNRAS*, 435, 502
- Fernández, R., Tchekhovskoy, A., Quataert, E., & et al. 2019, *MNRAS*, 482, 3373
- Frebel, A., & Ji, A. P. 2023, *Handbook of Nuclear Physics – Part III*, doi:10.48550/arXiv.2302.09188
- Freundlich, J., & Maoz, D. 2021, *MNRAS*, 502, 5882
- Fujimoto, S.-i., Hashimoto, M.-a., Kotake, K., & et al. 2007, *ApJ*, 656, 382
- Galadage, S., Adamcewicz, C., Zhu, X.-J., Stevenson, S., & Thrane, E. 2021, *ApJL*, 909, L19
- Halevi, G., & Mösta, P. 2018, *MNRAS*, 477, 2366
- Horowitz, C. J., Arcones, A., Côté, B., & et al. 2019, *J. Phys. G: Nucl. Part. Phys.*, 46, 083001
- Hotokezaka, K., Beniamini, P., & Piran, T. 2018, *Int. J. Mod. Phys. D*, 27, 1842005
- Hotokezaka, K., Kyutoku, K., Tanaka, M., & et al. 2013, *ApJL*, 778, L16
- Hotokezaka, K., Piran, T., & Paul, M. 2015, *Nat. Phys.*, 11, 1042
- Hotokezaka, K., Piran, T., & Paul, M. 2015, *Nature Physics*, 11, 1042
- Huth, S., Pang, P. T. H., Tews, I., et al. 2022, *Nature*, 606, 276
- Ivanova, N., Belczynski, K., Kalogera, V., Rasio, F. A., & Taam, R. E. 2003, *ApJ*, 592, 475
- Ji, A. P., Frebel, A., Chiti, A., & et al. 2016, *Nature*, 531, 610
- Just, O., Bauswein, A., Pulpillo, R. A., & et al. 2015, *MNRAS*, 448, 541
- Kedia, A., Ristic, M., O’Shaughnessy, R., et al. 2023, *Physical Review Research*, 5, 013168
- Kirby, E. N., Duggan, G., Ramirez-Ruiz, E., & et al. 2020, *ApJL*, 891, L13
- Kirby, E. N., Ji, A. P., & Kovalev, M. 2023, *ApJ*, 958, 45
- Kiuchi, K., Fujibayashi, S., Hayashi, K., & et al. 2023, *PhRvL*, 131, 011401
- Krüger, C. J., & Foucart, F. 2020, *Physical Review D*, 101, 103002
- Legred, I., Chatziioannou, K., Essick, R., Han, S., & Landry, P. 2021, *Physical Review D*, 104, 063003
- Lian, J., Storm, N., Guiglion, G., & et al. 2023, *MNRAS*, 525, 1329
- Macias, P., & Ramirez-Ruiz, E. 2018, *ApJ*, 860, 89
- Macias, P., & Ramirez-Ruiz, E. 2018, *ApJ*, 860, 89
- Madau, P., & Fragos, T. 2017, *ApJ*, 840, 39
- Maoz, D., & Graur, O. 2017, *ApJ*, 848, 25
- Mapelli, M., & Giacobbo, N. 2018, *MNRAS*, 479, 4391
- Margutti, R., & Chornock, R. 2021, *ARA&A*, 59, 155
- Matteucci, F., Romano, D., Arcones, A., Korobkin, O., & Rosswog, S. 2014, *MNRAS*, 438, 2177
- McMillan, P. J. 2011, *MNRAS*, 414, 2446
- Metzger, B. D. 2020, *Living Rev. Relativ.*, 23, 1
- Metzger, B. D., Martínez-Pinedo, G., Darbha, S., & et al. 2010, *MNRAS*, 406, 2650
- Metzger, B. D., Piro, A. L., & Quataert, E. 2008, *MNRAS*, doi:10.1111/j.1365-2966.2008.13789.x
- Metzger, B. D., Thompson, T. A., & Quataert, E. 2018, *ApJ*, 856, 101
- Naidu, R. P., Ji, A. P., Conroy, C., & et al. 2022, *ApJL*, 926, L36
- Nedora, V., Schianchi, F., Bernuzzi, S., & et al. 2021, *Class. Quantum Gravity*, 39, 015008
- Neijssel, C. J., Vigna-Gómez, A., Stevenson, S., et al. 2019, *MNRAS*, 490, 3740
- Nishimura, N., Sawai, H., Takiwaki, T., & et al. 2017, *ApJL*, 836, L21
- Nishimura, S., Kotake, K., Hashimoto, M.-a., & et al. 2006, *ApJ*, 642, 410
- Nugent, A. E., Fong, W.-f., Castrejon, C., et al. 2024, *ApJ*, 962, 5
- Oechslin, R., Janka, H.-T., & Marek, A. 2007, *A&A*, 467, 395
- Perego, A., Rosswog, S., Cabezón, R. M., & et al. 2014, *MNRAS*, 443, 3134
- Pian, E. 2021, *Front. Astron. Space Sci.*, 7, 108
- Piran, T. 1992, *ApJL*, 389, L45
- Pruet, J., Woosley, S. E., & Hoffman, R. D. 2003, *ApJ*, 586, 1254
- Radice, D., Bernuzzi, S., & Perego, A. 2020, *Annu. Rev. Nuc. Part. Sci.*, 70, 95
- Rastinejad, J. C., Gompertz, B. P., Levan, A. J., et al. 2022, *Nature*, 612, 223
- Reichert, M., Obergaulinger, M., Eichler, M., & et al. 2021, *MNRAS*, 501, 5733

- Roederer, I. U., Mateo, M., Bailey, III, J. I., & et al. 2016, *Monthly Notices of the Royal Astronomical Society*, 455, 2417
- Roederer, I. U., & Sneden, C. 2011, *The Astronomical Journal*, 142, 22
- Romero-Shaw, I. M., Farrow, N., Stevenson, S., Thrane, E., & Zhu, X.-J. 2020, *MNRAS*, 496, L64
- Rosswog, S., Liebendörfer, M., Thielemann, F.-K., & et al. 1999, *A&A*, 341, 499
- Ruffert, M., Janka, H.-T., Takahashi, K., & et al. 1997, *A&A*, 319, 122
- Salafia, O. S., Ravasio, M. E., Ghirlanda, G., & Mandel, I. 2023, *A&A*, 680, A45
- Siegel, D. M. 2019, *Eur. Phys. J. A*, 55, 203
- . 2022, *Nat. Rev. Phys.*, 4, 306
- Siegel, D. M., Barnes, J., & Metzger, B. D. 2019, *Natur*, 569, 241
- Siegel, D. M., Ciolfi, R., & Rezzolla, L. 2014, *ApJL*, 785, L6
- Siegel, D. M., & Metzger, B. D. 2017, *PhRvL*, 119, 231102
- Skúladóttir, Á., Hansen, C. J., Salvadori, S., & et al. 2019, *A&A*, 631, A171
- Suda, T., Yamada, S., Katsuta, Y., et al. 2011, *MNRAS*, 412, 843
- Surman, R., McLaughlin, G. C., & Hix, W. R. 2006, *ApJ*, 643, 1057
- Tarumi, Y., Hotokezaka, K., & Beniamini, P. 2021, *ApJL*, 913, L30
- The LIGO Scientific Collaboration, The Virgo Collaboration, The KAGRA Collaboration, & et al. 2021, *arXiv:2111.03606*, *arxiv:2111.03606*
- Van Der Swaelmen, M., Viscasillas Vázquez, C., Cescutti, G., & et al. 2023, *A&A*, 670, A129
- Wallner, A., Faestermann, T., Feige, J., & et al. 2015, *Nature Communications*, 6, 5956
- Wanderman, D., & Piran, T. 2015, *MNRAS*, 448, 3026
- Wehmeyer, B., Pignatari, M., & Thielemann, F. K. 2015, *MNRAS*, 452, 1970
- Winteler, C., Käppeli, R., Perego, A., & et al. 2012, *ApJL*, 750, L22
- Zevin, M., Kremer, K., Siegel, D. M., & et al. 2019, *ApJ*, 886, 4
- Zevin, M., Nugent, A. E., Adhikari, S., et al. 2022, *ApJL*, 940, L18